Nonperturbative transverse mode coupling in high-order harmonic generation

Martin Luttmann [1,*] Mekha Vimal [1] Matthieu Guer,[1,2] Titouan Gadeyne,[1,3] Céline Chappuis,[1]
Jean-François Hergott,[1] and Thierry Ruchon[1,†]

[1] *Université Paris-Saclay, CEA, CNRS, LIDYL, 91191 Gif-sur-Yvette, France*

[2] *Grupo de Investigación en Aplicaciones del Láser y Fotónica, Departamento de Física Aplicada, University of Salamanca, Salamanca 37008, Spain*

[3] *Département de Chimie, École Normale Supérieure, PSL University, 75005 Paris, France*

(Received 13 March 2023; accepted 4 October 2023; published 16 November 2023)

This paper is a joint publication with the paper by Vimal *et al.* [Phys. Rev. Lett. **131**, 203402 (2023)]. High-order harmonic generation (HHG) is an extreme nonlinear optical phenomenon at the heart of modern ultrafast physics. When HHG is driven by two noncollinear beams, one being significantly weaker than the other, the yields of the harmonic emission channels obey a perturbative power law with respect to the drivers' intensity ratio, even though HHG has a nonperturbative efficiency in general. Here, we drive HHG with two different transverse modes and show this power law to be directly imprinted in the spatial structure of the harmonic beamlets. As the driving beam intensities are brought closer, changes in the beamlet profiles reflect a transition from a perturbative to a nonperturbative behavior, understood by generalizing the photon-pathway formalism introduced in the companion paper. This work provides a visual method to study the efficiency of nonlinear optical processes and paves the way for finer all-optical shaping of extreme ultraviolet light.

DOI: 10.1103/PhysRevA.108.053509

I. INTRODUCTION

High-order harmonic generation (HHG) in gases is a highly nonlinear strong-field optical process which is nowadays routinely used to convert infrared (IR) radiation into trains of extreme ultraviolet (EUV) pulses with attosecond duration [1]. In the past two decades, these ultrashort light pulses have been used to probe the dynamics of electrons in atoms, molecules, and solids at their natural timescale. In the frequency domain, the HHG emission takes the form of a comb of odd harmonics of the fundamental IR frequency [2,3]. The process is usually explained with a semiclassical approach in which the driving field is a strong classical wave distorting the atomic potential of the gas atoms [4]. In this distorted potential, an outer electron successively undergoes tunnel ionization, acceleration in the continuum, and recombination with the parent ion accompanied by the emission of a burst of EUV radiation.

The HHG spectrum exhibits a characteristic plateau, as a broad range of harmonic orders are emitted with similar efficiency: in practice, the yield of a harmonic order q within the plateau region is approximated as $A^{q_{\mathrm{eff}}}$, where A is the strength of the driving field and q_{eff} is an effective nonlinearity order, roughly independent of q in the plateau [5,6]. This is in contrast to the processes of *perturbative* nonlinear optics [7], for which this exponent is equal to the number of input photons exchanged to generate a photon at the new frequency (which would predict $q_{\mathrm{eff}} = q$ for HHG). Despite this *nonperturbative* nature, HHG is often pictured as a parametric process involving the absorption of a well-defined number of photons from the driving beams and emission of an EUV photon—an image that proved particularly useful in understanding the conservation of various properties of the photon in HHG, such as its spin and orbital angular momenta [8–10]. In addition, it was shown that when HHG is driven by two noncollinear IR beams [11–18], one being significantly less intense than the other, the EUV emission can be interpreted with the tools of perturbative nonlinear optics [19,20]. In such an experiment, each harmonic separates angularly into several beamlets originating from the absorption of a different number of photons in each beam, and the yield of a beamlet involving p photons from the weak beam follows a α^p power law, where $\alpha = |E_2/E_1|$ is the amplitude ratio of the two driving fields. However, deviations from this perturbative-yield scaling law were rapidly observed as α increases, challenging the underlying parametric interpretation. Investigating the high-α regime, we proposed in the companion paper [21] a description that fully reproduces these deviations while still lending itself to both a field-based and a photon-based understanding.

In this paper, we drive HHG with two spatially structured noncollinear beams and show that for low values of α, the perturbative power law leaves a trace on the transverse profile of the emitted EUV radiation; that is, it can be directly deduced from an image of the far-field harmonics. The high-order harmonic channels can be expressed as powers of the driving transverse amplitudes and obey two-dimensional parity conservation. Upon increasing the intensity of the second beam, we observe changes in the spatial structure of the beamlets, hinting at deviations from the perturbative power law. The results broaden the scope of the photon-pathway framework introduced in Ref. [21], demonstrating that it can be generalized to predict not only the yields but also the spatial modes of the harmonic beamlets.

*martin.luttmann@cea.fr
†thierry.ruchon@cea.fr

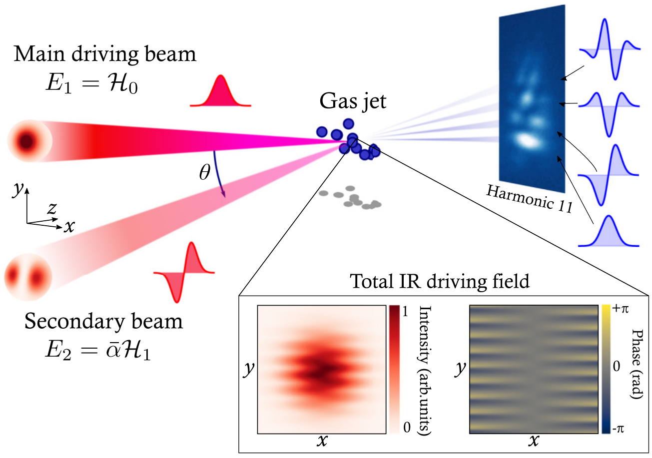

FIG. 1. Principle of noncollinear HHG with different transverse modes in the driving beams. Here, the main IR beam is a Gaussian mode, and the weak secondary beam is a $\mathcal{H}_{1,0}$ mode. At the crossing point, the intensity and phase of the IR field exhibit a gratinglike structure. The generated harmonic beamlets are separated angularly, as dictated by conservation of the linear momentum of the absorbed photons. Each beamlet is observed to have a specific transverse profile.

II. HHG DRIVEN BY TWO STRUCTURED BEAMS

As further detailed in the companion paper [21], an analytical development of the so-called *thin-slab model* (TSM) of HHG [6] can be used to derive the yield of the beamlets; we show here that this formalism extends to predicting their transverse profiles. We consider two beams crossing with a small relative angle θ, both linearly polarized in the same direction (neglecting the small longitudinal polarization components). Beam 1 propagates along z with wave vector $\vec{k}_1$, and its transverse profile at the crossing point is given by the complex scalar field $E_1(x, y)$. Beam 2 propagates in the y-z plane with wave vector $\vec{k}_2$, and its transverse profile at the crossing point is given by $E_2(x, y)e^{i\Delta k^\perp y}$, where $\Delta k^\perp = (\vec{k}_2 - \vec{k}_1)\cdot\hat{y}$ (see Fig. 1). The total field at their crossing is

$$E(x, y) = E_1(x, y) + E_2(x, y)e^{i\Delta k^\perp y}. \tag{1}$$

From here on, we drop the (x, y) dependence of the fields. In the TSM, the harmonic near field is given by

$$E_q^{\mathrm{nf}} = |E|^{q_{\mathrm{eff}}} e^{iq \arg[E]}. \tag{2}$$

In our experimental conditions, the effective nonlinearity order of HHG is $q_{\mathrm{eff}} \approx 3.5$ [6]. For positions (x, y) of the generating plane where $|E_2| < |E_1|$, the harmonic field is rewritten as (see Appendix B)

$$E_q^{\mathrm{nf}} = |E_1|^{q_{\mathrm{eff}}} \sum_{p=-\infty}^{+\infty} e^{ip\Delta k^\perp y} e^{i(q-p)\arg[E_1]} e^{ip\arg[E_2]} \times \sum_{n=0}^{+\infty} \left|\frac{E_2}{E_1}\right|^{|p|+2n} a_p^n, \tag{3}$$

with $a_p^n = \binom{q^+}{n+\frac{|p|+p}{2}}\binom{q^-}{n+\frac{|p|-p}{2}}$, where $\binom{s}{n} = \prod_{m=0}^{n-1}(s-m)/n!$ are generalized binomial coefficients. We also introduced $q^\pm = \frac{q_{\mathrm{eff}}\pm q}{2}$. In the above expression, each value of p corresponds to a beamlet of harmonic q in the far field, emitted at angle $p\theta/q$, that can be understood, from linear-momentum conservation, as coming from the net absorption of p photons from beam 2.

In the perturbative limit, that is, when the power of beam 2 is much lower than that of beam 1, Eq. (3) alone approximates well the harmonic field: indeed, the validity condition $|E_2(x, y)| < |E_1(x, y)|$ is held in most regions of high laser intensity which effectively contribute to the harmonic emission. Keeping only the leading term in the power series, the transverse amplitude of beamlet p is expressed as

$$E_q^p \propto e^{i(q-p)\arg[E_1]} e^{ip\arg[E_2]} |E_1|^{q_{\mathrm{eff}}-|p|} |E_2|^{|p|}. \tag{4}$$

From this formula, HHG may be described as behaving *perturbatively* with respect to the weak secondary beam (with which $|p|$ photons are exchanged) and *nonperturbatively* with respect to the main one, which retains a q_{eff} power scaling. We remark that the phase of beamlet p is built from $q - p$ times that of the first beam and p times that of the second, in perfect agreement with a photon-pathway picture, with demonstrated orbital angular momentum up-conversion rules in noncollinear high-order harmonic generation (NCHHG) [9].

The corresponding far-field transverse amplitude is then computed as the Fourier transform of Eq. (4). With two driving beams having the same transverse envelope ($E_1 = \alpha E_2$ for all x, y), no effect on the transverse amplitude is expected: all beamlets have the same profile $|E_1|^{q_{\mathrm{eff}}}$, as can be seen in the companion paper in the case of two identical Gaussian beams [21]. However, using two differently structured light beams, for instance, distinct Hermite-Gaussian (HG) modes [22], we expect the beamlets to exhibit different transverse-amplitude profiles, as an imprint left by the perturbative power law (Fig. 1). As the magnitude of E_2 is increased, additional terms become important in Eq. (3), and transverse profiles should evolve accordingly. Note that since the two driving beams do not have the same transverse profile, the ratio $|E_2/E_1|$ now varies in space. In the following we will instead use the ratio $\bar{\alpha} = \sqrt{P_2/P_1}$, where P_2 and P_1 are the powers of each IR beam, as measured experimentally with a power meter.

To verify these predictions, we drive HHG with two noncollinear beams, one being Gaussian and the other being a HG mode. HG beams are transverse modes in free space that naturally emerge when solving the propagation equation in Cartesian coordinates [22]. They are determined by two indices, j and m, describing the number of amplitude nodes in the two spatial directions. In this work we consider only the case where the vertical index is null, i.e., modes of the type $\mathcal{H}_{j,0}$, although the results can be generalized to two-dimensional HG modes. To make the notations more concise, we drop the second index. In this frame, the electric field of the HG modes at the focus ($z = 0$) is written as

$$\mathcal{H}_j(x/w_0) = C_j H_j\left(\frac{\sqrt{2}x}{w_0}\right) e^{-(x/w_0)^2}, \tag{5}$$

with w_0 being the beam waist. H_j are the Hermite polynomials, in their physics definition, and $C_j = (2/\pi)^{\frac{1}{4}}/\sqrt{2^j j!}$ is a normalization factor.

III. EXPERIMENTAL RESULTS

We perform the following experiment, depicted in Fig. 1. We drive HHG with a Ti:Sa laser delivering pulses of 25-fs duration and 1.3-mJ energy at an 800-nm wavelength. The beam is divided into two arms in a Mach-Zehnder interferometer with a 50:50 beam splitter. A set with a half-wave plate and a polarizer allows us to adjust the intensity of the secondary beam. A phase plate with a π step is used to convert the secondary beam into a $\mathcal{H}_1$ mode at focus. The two beams are focused by 75-cm focal-length lenses, then recombined noncollinearly, and overlapped temporally and spatially at the output of the interferometer. Their relative angle is $\theta = 24$ mrad. Harmonics are generated at the focus of the IR beams in a jet of argon gas. The gas jet is located slightly downstream of the focal points of the laser beams, so that long-trajectory contributions can be neglected [23]. In order to resolve the transverse harmonic profile, we use a near-normal incidence spectrometer consisting of a refocusing spherical mirror (600-mm curvature radius) and a normal-incidence grating. The harmonic intensity is finally recorded with a set of microchannel plates and a phosphor screen, imaged by a CCD camera. Figure 2(a) shows the far-field intensity of harmonic $q = 11$ for a ratio of the driving pulse energies $\bar{\alpha} \approx 0.17$. The harmonic beamlets all have different profiles, exhibiting $|p| + 1$ horizontal intensity lobes. This observation is a telltale signature of the perturbative power law of Eq. (4). To see why, let us consider a Gaussian beam $E_1 = \mathcal{H}_0(x/w_0)$ and the HG mode $E_2 = \bar{\alpha}\mathcal{H}_1(x/w_0)$ in Eq. (4). The near-field horizontal profile of the pth beamlet is given by

$$E_q^p \propto |E_1|^{q_{\text{eff}}} \left[\frac{E_2}{E_1}\right]^{|p|} \propto e^{-q_{\text{eff}}(x/w_0)^2} \left[H_1\left(\frac{\sqrt{2}x}{w_0}\right)\right]^{|p|}. \tag{6}$$

The H_1 polynomial raised to the power $|p|$ can be expressed as a superposition of Hermite polynomials with an order inferior or equal to $|p|$ and of the same parity as $|p|$ [24], yielding a decomposition of the form (see Appendix B)

$$E_q^p \propto \sum_{m=0}^{\lfloor |p|/2 \rfloor} g_{|p|-2m}^{(p)} \mathcal{H}_{|p|-2m}\left(\frac{x\sqrt{q_{\text{eff}}}}{w_0}\right). \tag{7}$$

Here, $g_j^{(p)}$ are coefficients of the HG mode decomposition, which take real and positive values. We propagate each $\mathcal{H}_j$ mode to the far field, taking into account the accumulated Gouy phase $(j+1)\pi/2$. Since our beamlets are superpositions of HG modes of the same parity, the propagation consists of simply imposing a π phase shift between successive HG components. In the far field, the pth beamlet is written as

$$\mathcal{F}\{E_q^p\}(u) \propto \sum_{m=0}^{\lfloor |p|/2 \rfloor} g_{|p|-2m}^{(p)} (-1)^m \mathcal{H}_{|p|-2m}\left(\frac{u}{w_\infty}\right) \tag{8}$$

$$\propto e^{-(u/w_\infty)^2} H_{|p|}\left(\frac{u}{w_\infty}\right), \tag{9}$$

where u is the horizontal far-field coordinate, dimensionally equivalent to a length (in Fig. 2, v denotes the corresponding vertical coordinate), and w_∞ is the waist of the beam in the detector plane. In fact (see Appendix B), this profile can also be described as a Gaussian envelope multiplied by a single Hermite polynomial of order $|p|$ (note that this does *not* make a pure HG mode due to the missing $\sqrt{2}$ in the argument of the polynomial). Accordingly, the beamlets in Fig. 2 feature $|p| + 1$ intensity peaks, but the outer peaks are less intense than they would be in pure HG modes. We decompose the transverse profiles in a series of HG modes by minimizing their root-mean-square distance to a sum of HG functions with real leading coefficients [Fig. 2(d)]. The experimental results are consistent with the TSM simulations results shown in Fig. 2(b). As expected from Eq. (8), beamlets $p = 0$ and $p = 1$ are pure HG modes, while higher beamlets are superpositions of HG modes of the same parity as p, with alternating signs. It must be noted that this field structure is in agreement with that observed in perturbative second-order harmonic generation driven by a HG mode [25].

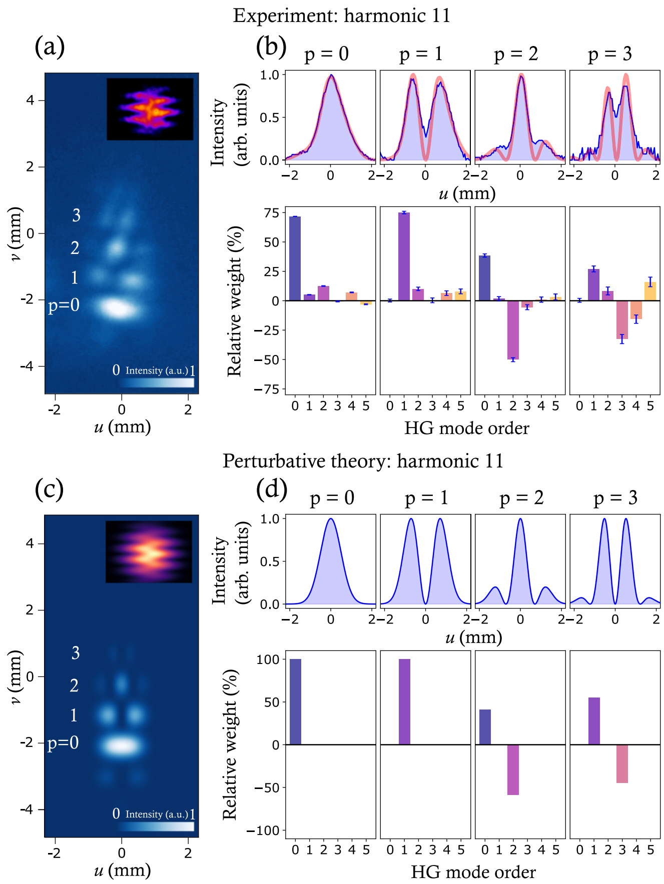

FIG. 2. (a) Experimental beamlet intensities for harmonic $q = 11$ driven by an intense Gaussian beam and a weak $\mathcal{H}_1$ mode in a noncollinear geometry for $\bar{\alpha} \approx 0.17$. The inset shows the intensity profile of the driving field. (b) Horizontal lineouts of the beamlets in (a) (top) and corresponding HG mode spectra (bottom) obtained by a fit of the intensity profiles. The best fit with a superposition of the first five HG modes is shown with red curves in the top row. The error bars correspond to the standard deviation associated with each of the five parameters of the fit. (c) Thin-slab simulation [Eq. (2)] of the experiment in (a) ($\bar{\alpha} \approx 0.17$). The inset shows the intensity profile of the driving field. (d) Horizontal intensity profiles (top) and HG mode spectra (bottom) of the first four beamlets, according to the perturbative law, Eq. (8).

To further validate our theory, we also performed the HHG experiment in two complementary situations: one in which

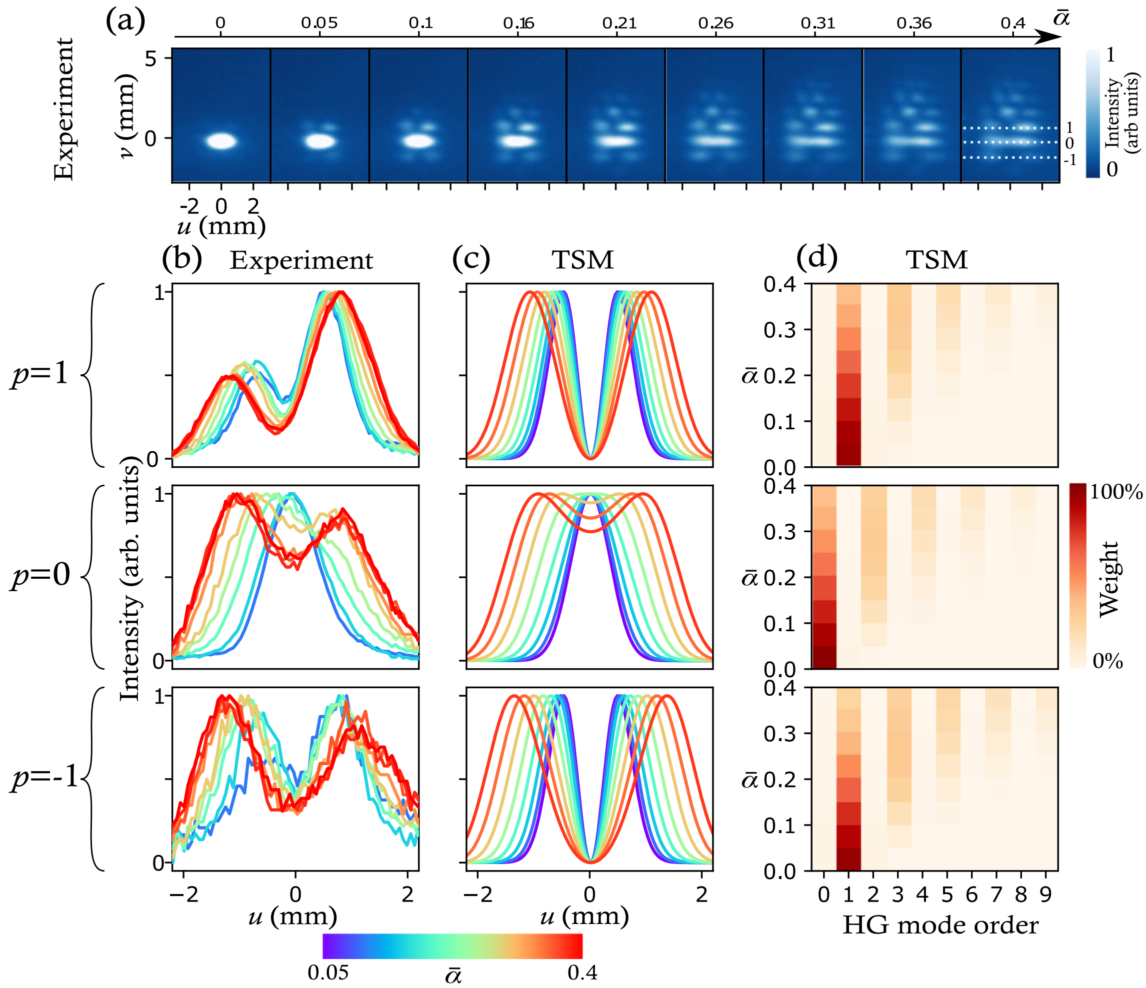

FIG. 3. (a) Far-field image of harmonic $q = 11$ as a function of the power ratio of the drivers, ranging from $\bar{\alpha} \approx 0.05$ to $\bar{\alpha} \approx 0.4$. (b) Horizontal lineouts of three beamlets ($p = 1, 0, -1$) in (a). (c) Normalized intensity profiles of the beamlets obtained by thin-slab simulations based on Eq. (2) for the same parameters as in the experiment. (d) HG mode decomposition of the profiles in (c) as a function of $\bar{\alpha}$.

the main beam is a $\mathcal{H}_1$ mode and the secondary beam is Gaussian and one in which both drivers are $\mathcal{H}_1$ modes (see Appendix A). In the first case, we observe a situation opposite to that in Fig. 2: the number of horizontal lobes in the profile decreases with increasing p, while the barycenter of the HG mode spectrum shifts toward zero. In the second case, both the density of lobes in the profile and the HG mode spectrum remain roughly constant with p, which agrees with a $(\mathcal{H}_1)^{q_{\text{eff}}-|p|}(\mathcal{H}_1)^{|p|} = (\mathcal{H}_1)^{q_{\text{eff}}}$ scaling.

We now broaden our scope, going beyond the perturbative limit. To do so, we increase the intensity of the secondary beam up to $\bar{\alpha} \approx 0.4$. Because of the strongly nonperturbative nature of HHG, we expect deviations from Eq. (4) that should be observable in the far-field amplitude of the beamlets. Figure 3 displays the results of this power scan. In Fig. 3(a), we show the intensity profile of harmonic $q = 11$ as a function of $\bar{\alpha}$: as it increases, more beamlets that all obey parity conservation show up. Horizontal lineouts of beamlets $p = 0$ and $p = \pm 1$ are shown in Fig. 3(b). We observe that the $p = 0$ beamlet starts from a Gaussian shape, then progressively elongates in the horizontal direction, and finally obtains a doubly-lobed profile. For beamlets $p \neq 0$, the profiles remain structurally similar, but the distance between intensity maxima increases. These qualitative features are well reproduced by TSM simulations [Fig. 3(c)]. The discrepancy between the TSM and experimental curves, in particular the observation of left-right asymmetry, is probably a consequence of slight misalignments of the two beams, gas target, and detection system, although we have not identified its precise origin thus far.

Using the present theory and observations, we can generalize the photon-pathway formalism introduced in the companion paper to account for the mode structure of the harmonic beamlets. Equation (3) suggests that for each beamlet p, we must identify all photon exchange processes that result in emission of a harmonic q photon at angle $p\theta/q$ and sum the associated amplitudes. In addition to the perturbative channel, which takes $q - p$ photons from the first beam and p from the second, there are higher-order pathways involving absorption and subsequent stimulated emission of photons in the secondary beam, as pictured in Fig. 4. Pathways involving the exchange of $|p| + 2n$ photons with beam 2 contribute

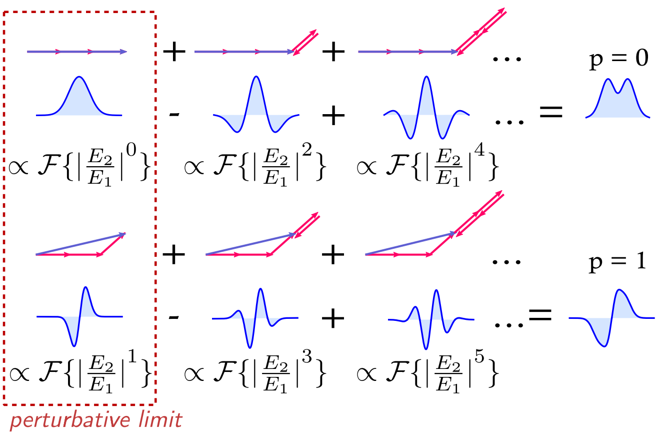

FIG. 4. Generalization of the photon-pathway formalism to spatial modes. Equation (3) formulates each beamlet as a power series, conveniently interpreted as a natural continuation of the parametric picture of HHG: photon pathways involving the exchange of $|p| + 2n$ photons with beam 2 add contributions beyond the leading perturbative term, with profiles scaling as $|E_2/E_1|^{|p|+2n}(x, y)$. Here, the total profiles are those observed for $\bar{\alpha} \approx 0.4$. Note that as $\bar{\alpha}$ is increased, the validity condition $|E_2/E_1|(x, y) < 1$ for using Eq. (3) is violated in more and more regions. However, the mirror formula for $|E_2/E_1|(x, y) > 1$ still has the same form of a series expansion, and the photon-pathway understanding remains valid, albeit with less trivial spatial envelopes, which become functions of $\bar{\alpha}$.

the term $\propto |E_2/E_1|^{|p|+2n}(x, y)$ to the series. This explains why the HG spectrum of the beamlets [Fig. 3(d)] exhibits growing contributions of the $|p| + 2n$ components. The sum of all pathways therefore determines both the yield and spatial profile of the beamlets. Figure 4 shows as an example the first three pathways contributing to beamlets $p = 0$ and $p = 1$. For $p = 0$, the amplitude of the leading term evidently has a Gaussian shape (from the global $|E_1|^{q_{\text{eff}}}$ factor). Higher-order contributions have more and more lobes and extend over a wider transverse range. As a result, they tend to elongate the beamlet profiles horizontally, as observed in both the experiment and simulation. For $p = 0$, contributions with negative values at the center tend to carve the Gaussian peak, producing the doubly-lobed profile observed in experiments for $\bar{\alpha} \approx 0.4$ and sketched in Fig. 4. Note that the existence of these additional contributions—and therefore the observations in Fig. 3—is a direct consequence of the nonperturbative nature of HHG: in the perturbative case where $q_{\text{eff}} = q$, the sum over n vanishes in Eq. (3), leaving only the perturbative leading term.

IV. CONCLUSION

In this study, we used transverse laser modes to monitor the transition between perturbative and nonperturbative behavior in the two-beam HHG process via spatial mode coupling in the EUV. The analysis of the far-field harmonic structure allowed us to deduce in a visual manner the previously reported perturbative power-law scaling when one of the two beams is much weaker than the other. For larger intensities in the second beam, we observed evolutions of the beamlet profiles as a direct consequence of the nonperturbative nature of HHG. These were interpreted by generalizing the framework introduced in the companion paper: each higher-order photon pathway that contributes to the yield can, in fact, be associated with a specific spatial envelope, and in summing all pathways we recover the observed transverse beamlet profiles.

These experiments and theoretical formalism pave the way for finer, all-optical control of the spatial mode structure of high-order harmonic beams. The experiment could be extended to other mode families, for instance, Laguerre-Gaussian (LG) modes [26,27] and Bessel beams [28], that carry orbital angular momentum (OAM). The power law would generate radial structures [29,30] in the far field which would be modified in a nonperturbative regime. In that spirit, we note that the $\mathcal{H}_1$ mode can be expressed as a sum of two LG modes with OAM $\ell = \pm 1$ [31] and thus that our results could possibly be seen through the prism of OAM conservation in HHG. Other developments could include beams with different frequencies, polarization states, or schemes involving more than two beams. The underlying parametric understanding calls for a quantum-optical theory of NCHHG that would explicitly involve the spatial modes of the driving photons. Finally, we emphasize that our approach provides a general method for investigating efficiency scaling laws in nonlinear optical phenomena: the same concepts could find use in other processes such as solid-state HHG [31] and four-wave mixing [7].

ACKNOWLEDGMENTS

The authors thank C. Hernández-García and L. Plaja for helpful discussions. This work was supported by the French "Investments for the Future" of the Agence Nationale pour la Recherche (Contracts No. 11-EQPX0005-ATTOLAB, No. ANR-14-CE32-0010-Xstase, No. ANR-10-LABX-0039-PALM ATTO-Foam, and No. ANR HELIMAG ANR-21-CE30-0037), by the Scientific Cooperation Foundation of Paris-Saclay University through the funding of the OPT2X research project (Lidex 2014), by the Île-de-France region through the Pulse-X project, and by the European Union's Horizon 2020 research and innovation program, Grant No. EU-H2020-LASERLAB-EUROPE-654148. The École Normale Supérieure (Paris) is gratefully acknowledged for T.G.'s fellowship.

APPENDIX A: ADDITIONAL EXPERIMENTAL DATA

In Fig. 5 we provide a camera image of the NCHHG beamlets for several harmonic orders. The qualitative observations made for $q = 11$ in the main text hold for other orders.

In Fig. 6 we present additional experimental data for NCHHG driven by a $\mathcal{H}_1$ mode in the main beam and either a Gaussian or another $\mathcal{H}_1$ mode in the secondary beam.

APPENDIX B: ANALYTICAL DERIVATIONS

1. Derivation of Eq. (3)

A detailed derivation of the photon-pathway formula given as Eq. (3) in the main text is described in the Supplemental Material of the companion paper, where it is listed as Eq. (5). The mirror formula for when $|E_2/E_1| > 1$ is listed as Eq. (6).

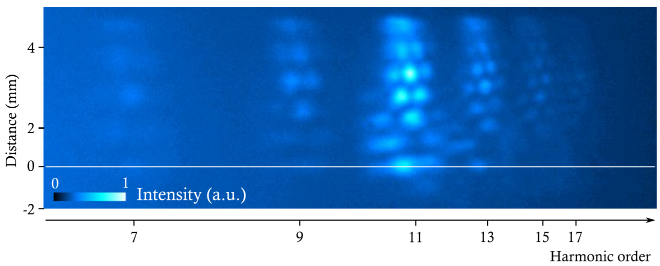

FIG. 5. Raw image recorded at the back of the MCP for a Gaussian main driving beam and a $\mathcal{H}_1$ secondary beam. It corresponds to $\bar{\alpha} \approx 0.8$ (the highest amplitude ratio that we could reach with our setup) to show many beamlets with the expected parities and clear deviations from the perturbative-regime profiles. The white horizontal line indicates the position of the $p = 0$ beamlet for all harmonics.

2. Derivation of Eqs. (7)–(9)

We now derive Eqs. (7)–(9). We start from Eq. (6) of the main text for the near field of beamlet p in the perturbative limit:

$$E_q^p \propto \left[H_1\left(\frac{\sqrt{2}x}{w_0}\right)\right]^{|p|} e^{-q_{\text{eff}}(x/w_0)^2}$$
$$= \left[\frac{2\sqrt{2}x}{w_0}\right]^{|p|} e^{-q_{\text{eff}}(x/w_0)^2}.$$

We use the inverse definition of the Hermite polynomials

$$x^n = \frac{n!}{2^n}\sum_{m=0}^{\lfloor n/2\rfloor}\frac{1}{m!(n-2m)!}H_{n-2m}(x)$$

to rewrite the field as a sum of Hermite polynomials with the argument $\sqrt{2}x/W$, where $W = w/\sqrt{q_{\text{eff}}}$ is the waist of the harmonic beam:

$$E_q^p = e^{-(x/W)^2}\sum_{m=0}^{\lfloor |p|/2\rfloor}\frac{\left[\frac{1}{\sqrt{q_{\text{eff}}}}\right]^{|p|}(|p|)!}{m!(|p|-2m)!}H_{|p|-2m}\left(\frac{\sqrt{2}x}{W}\right)$$
$$= \sum_{m=0}^{\lfloor |p|/2\rfloor}\frac{\left[\frac{1}{\sqrt{q_{\text{eff}}}}\right]^{|p|}(|p|)!}{m!(|p|-2m)!}\frac{1}{C_{|p|-2m}}\mathcal{H}_{|p|-2m}\left(\frac{x}{W}\right)$$
$$= \sum_{m=0}^{\lfloor |p|/2\rfloor} g_{|p|-2m}^{(p)}\mathcal{H}_{|p|-2m}\left(\frac{x}{W}\right).$$

This is Eq. (7) from the main text. $\mathcal{H}_j$ are eigenmodes of paraxial propagation, and upon Fourier transformation to the far field, they differ by only the accumulation of a Gouy phase $(j+1)\pi/2$:

$$\mathcal{F}\{E_q^p\} \propto \sum_{m=0}^{\lfloor |p|/2\rfloor} g_{|p|-2m}^{(p)} e^{i(|p|-2m+1)\pi/2}\mathcal{H}_{|p|-2m}\left(\frac{u}{w_\infty}\right)$$
$$\propto \sum_{m=0}^{\lfloor |p|/2\rfloor} g_{|p|-2m}^{(p)}(-1)^m\mathcal{H}_{|p|-2m}\left(\frac{u}{w_\infty}\right),$$

where u is the horizontal coordinate in the far field and w_∞ is the beam waist in the far field. The formula above is Eq. (8) from the main text.

For $\gamma \in \mathbb{R}$, the Hermite polynomials obey the following scaling property:

$$H_j(\gamma x) = \sum_{n=0}^{\lfloor j/2\rfloor}\gamma^{j-2n}(\gamma^2-1)^n\binom{j}{2n}\frac{(2n)!}{n!}H_{j-2n}(x).$$

Recalling the expression of the $g_j^{(p)}$ coefficients, we can make use of this theorem with $\gamma = 1/\sqrt{2}$ to rewrite the profile as

$$\mathcal{F}\{E_q^p\} \propto e^{-(u/w_\infty)^2}\sum_{m=0}^{\lfloor |p|/2\rfloor}\frac{(-1)^m(|p|)!}{m!(|p|-2m)!}H_{|p|-2m}\left(\frac{\sqrt{2}u}{w_\infty}\right)$$
$$\propto e^{-(u/w_\infty)^2}H_{|p|}\left(\frac{u}{w_\infty}\right),$$

which is Eq. (9) of the main text.

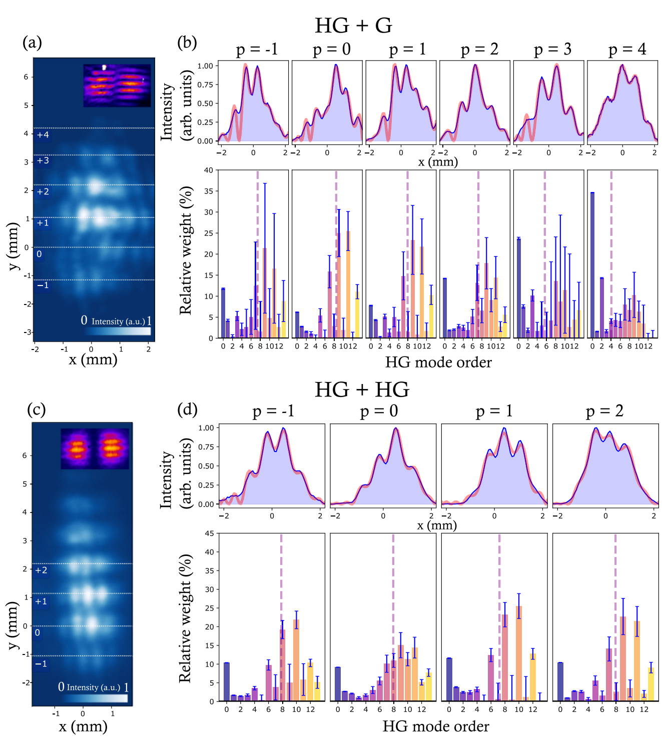

FIG. 6. (a) Intensity profile of harmonic $q = 11$ with a $\mathcal{H}_1$ main driving beam and Gaussian secondary beam. The digits indicate the order p of each beamlet. The inset image displays the IR intensity at focus. (b) Top: lineouts along the horizontal lines in (a) (blue) and the best fit with the sum of the first ten HG modes (red lines). Bottom: corresponding HG mode decompositions. The vertical dashed line indicates the barycenter of the spectrum. (c) Intensity profile of harmonic $q = 11$ with the same $\mathcal{H}_1$ mode in both the main beam and the secondary beam. The inset displays the IR intensity at focus. (d) Top: lineouts along the horizontal lines in (c) (blue) and the best fit with the sum of the first ten HG modes (red lines). Bottom: corresponding HG mode decomposition.

3. Alternative derivation of Eq. (9)

In this section, we provide an alternative derivation of the beamlet profiles in the perturbative regime, Eq. (9) of the main text. Here, instead of using the photon-pathway series expansion, we adopt a more "wave-based" approach by applying the small-$\bar{\alpha}$ approximation to the amplitude and phase of the driving field separately and plugging the results in the thin-slab formula.

We consider NCHHG driven by a Gaussian on-axis laser beam (wave vector $\mathbf{k}_1 = k\mathbf{u}_z$) and a weak $\mathcal{H}_1$ mode (wave vector $\mathbf{k}_2 = k\cos\theta\mathbf{u}_z + k\sin\theta\mathbf{u}_y$) coming at an angle θ. The two drivers lie in the vertical yz plane. In the following, we consider that HHG occurs in an infinitely thin plane located at $z = 0$. The electric fields of the beams read

$$E_1(x, y) = e^{-r^2/w_0^2} e^{i\mathbf{k}_1\cdot\mathbf{r}} = e^{-r^2/w_0^2},$$

$$E_2(x, y) = \bar{\alpha}C_1 \frac{2\sqrt{2}x}{w_0} e^{-(x^2\cos^2\theta + y^2)/w_0^2} e^{i\mathbf{k}_2\cdot\mathbf{r}} = \bar{\alpha}C_1 \frac{2\sqrt{2}x}{w_0} e^{-(x^2\cos^2\theta + y^2)/w_0^2} e^{iky\sin\theta},$$

where $\mathbf{r} = x\mathbf{u}_x + y\mathbf{u}_y$ is the position vector in the transverse plane, $r = |\mathbf{r}|$, and C_1 is a normalization constant for the $\mathcal{H}_1$ mode.

Approximation 1. In practice, θ is of the order of a few tens of milliradians. $\theta \ll 1$ allows us to merge the transverse planes of the two beams: $\cos\theta \approx 1$ in the above formula, and we assume $\sin\theta \approx \theta$. The total field is given by

$$E_s(\mathbf{r}) \approx e^{-r^2/w_0^2}\left(1 + \bar{\alpha}C_1 \frac{2\sqrt{2}x}{w_0} e^{-iky\theta}\right).$$

The amplitude and phase of this field are

$$|E_s(x, y)| = e^{-\frac{r^2}{w_0^2}} \sqrt{1 + \bar{\alpha}C_1 \frac{4\sqrt{2}x}{w_0}\cos(ky\theta) + 8(\bar{\alpha}C_1)^2 \frac{y^2}{w_0^2}},$$

$$\varphi(x, y) = \tan^{-1}\left(\frac{\bar{\alpha}C_1 \frac{2\sqrt{2}x}{w_0}\sin(ky\theta)}{1 + \bar{\alpha}C_1 \frac{2\sqrt{2}x}{w_0}\cos(ky\theta)}\right). \tag{B1}$$

Approximation 2. We consider the secondary beam to be much weaker than the main one (perturbative regime); hence, $\bar{\alpha} \ll 1$. At first order, the modulus and phase of the total field simplify to

$$|E_s(x, y)| \approx e^{-r^2/w_0^2}\left(1 + \bar{\alpha}C_1 \frac{2\sqrt{2}x}{w_0}\cos(ky\theta)\right),$$

$$\varphi(x, y) \approx \bar{\alpha}C_1 \frac{2\sqrt{2}x}{w_0}\sin(ky\theta). \tag{B2}$$

Approximation 3. We approximate one step further and neglect the term linear in $\bar{\alpha}$ in Eq. (B2),

$$|E_s(x, y)| \approx e^{-r^2/w_0^2}. \tag{B3}$$

This is the same as assuming that all the information on the active grating structure is encapsulated in the phase φ. Using these results in the thin-slab formula [Eq. (2) of the main text] and taking the two-dimensional Fourier transform, we obtain the far-field amplitude of harmonic q,

$$A^q(u', v') = \iint dxdy e^{iq\bar{\alpha}C_1 \frac{2\sqrt{2}x}{w_0}\sin(ky\theta)} \times e^{-q_{\text{eff}}r^2/w_0^2} e^{-i(u'x+v'y)},$$

where $u' = \frac{kqu}{D}$ and $v' = \frac{kqv}{D}$, with u and v being the horizontal and vertical coordinates in the far-field transverse plane, located at a large distance D from the focus. In order to compute this integral, we use the Jacobi-Anger identity to write the phase term as a sum of Bessel functions:

$$e^{iq\bar{\alpha}C_1 \frac{2\sqrt{2}x}{w_0}\sin(ky\theta)} = \sum_{p=-\infty}^{+\infty} J_p\left(q\bar{\alpha}C_1 \frac{2\sqrt{2}x}{w_0}\right) e^{ipky\theta},$$

with J_p being the pth Bessel function of the first kind. The pth term of the sum corresponds to the pth beamlet of harmonic order q. The amplitude can now be written as a product of two integrals on the separate variables x and y:

$$A^q(u', v') = \sum_{m=-\infty}^{+\infty} \overbrace{\int dy e^{-q_{\text{eff}}y^2/w_0^2} e^{iy(pk\theta - v')}}^{I_y^p(v')} \times \underbrace{\int dx J_p\left(q\bar{\alpha}C_1 \frac{2\sqrt{2}x}{w_0}\right) e^{-q_{\text{eff}}x^2/w_0^2} e^{-iu'x}}_{I_x^p(u')}.$$

$I_y^p(v')$ corresponds to the profile of the pth beamlet along the vertical coordinate v. We have

$$I_y^p(v') = w_0\sqrt{\frac{\pi}{q_{\text{eff}}}} \exp\left(-\frac{w_0^2}{4q_{\text{eff}}}(v' - pk\theta)^2\right).$$

As expected, the profile of the pth beamlet in the v (vertical) direction is given by a Gaussian function emitted at an angle $v/D = p\theta/q$. Let us now consider the second integral, $I_x^p(u)$. It gives the profile of the pth beamlet along the horizontal coordinate u. For convenience, we rewrite the integral in a simpler form,

$$I_x^p(U) = \frac{w_0}{q\bar{\alpha}C_1 2\sqrt{2}} \int dX J_p(X) e^{-aX^2} e^{-iUX},$$

with $X = q\bar{\alpha}C_1 2\sqrt{2}x/w_0$, $U = w_0u'/(2\sqrt{2}q\bar{\alpha}C_1)$, and $a = q_{\text{eff}}/(8q^2\bar{\alpha}^2C_1^2)$.

Approximation 4. We have $\bar{\alpha} \ll 1$, so $X \ll 1$. In addition, the e^{-aX^2} factor will tend to suppress the near-field amplitude when $q_{\text{eff}}x^2/w_0^2$ is not negligible compared to 1. For those reasons, we can consider that the only appreciable contribution in $I_x^p(U)$ comes from the neighborhood of $x = 0$. We can therefore use the well-known approximation of the Bessel functions

$$J_{p\geqslant 0}(X \ll 1) \approx \left(\frac{X}{2}\right)^p \frac{1}{\Gamma(p+1)},$$

with Γ being the Euler integral of the second kind, such that $\Gamma(p+1) = p!$. The validity of this approximation is illustrated in Fig. 7. Note that it also holds for negative diffraction orders (i.e., for $p < 0$) by using the appropriate expression

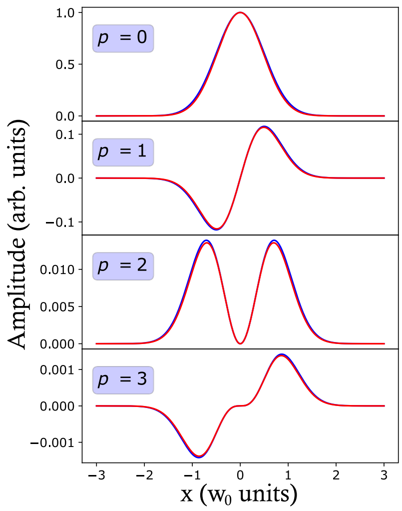

FIG. 7. Comparison between the exact near-field amplitude $J_p(X)e^{-aX^2}$ of Eq. (B3) (red lines) and the approximation using Eq. (B3) (blue lines) for $\bar{\alpha} = 0.05$, $q_{\rm eff} = 3.5$, and $q = 11$ for different beamlets p.

$J_{p<0}(X \ll 1) \approx (\frac{2}{X})^p \frac{(-1)^p}{(-p)!}$. The integral thus becomes

$$I_x^p(U) = \frac{w_0}{q\bar{\alpha}C_1 2\sqrt{2}} \frac{2^{-p}}{p!} \int dX X^p e^{-aX^2} e^{-iUX}$$

$$= \frac{w_0}{q\bar{\alpha}C_1 2\sqrt{2}} \frac{1}{p!} \left(\frac{i}{2}\right)^p \frac{d^p}{dU^p} \int dX e^{-aX^2} e^{-iUX}$$

$$= \frac{w_0}{q\bar{\alpha}C_1 2\sqrt{2}} \frac{\sqrt{\pi/a}}{p!} \left(\frac{i}{2}\right)^p \frac{d^p}{dU^p} \left(e^{-U^2/4a}\right).$$

This last formula is, up to an inverse Gaussian prefactor, the definition of the Hermite polynomials. Indeed, $\forall K \in \mathbb{R}$,

$$H_p(K) = (-1)^p e^{K^2} \frac{d^p}{dK^p} e^{-K^2}.$$

So we can finally write

$$I_x^p(U) = \frac{w_0}{q\bar{\alpha}C_1 2\sqrt{2}} \frac{\sqrt{\pi/a}}{p!} \left(\frac{-i}{2\sqrt{a}}\right)^p e^{-U^2/4a} H_p(U/2\sqrt{a}).$$

Coming back to the previous notations, we get

$$I_x^p(u') = \frac{w_0\sqrt{\pi}}{\sqrt{q_{\rm eff}}\, p!} \left(\frac{-i\sqrt{2}q\bar{\alpha}C_1}{2\sqrt{q_{\rm eff}}}\right)^p e^{-\frac{w_0^2 u'^2}{4q_{\rm eff}}} H_p\left(\frac{w_0 u'}{2\sqrt{q_{\rm eff}}}\right)$$

$$= \frac{w_0\sqrt{\pi}}{\sqrt{q_{\rm eff}}\, p!} \left(\frac{-i\sqrt{2}q\bar{\alpha}C_1}{2\sqrt{q_{\rm eff}}}\right)^p e^{-\frac{w_0^2 (kqu)^2}{4q_{\rm eff}D^2}} H_p\left(\frac{w_0 kqu}{2D\sqrt{q_{\rm eff}}}\right).$$

The horizontal profile of the pth beamlet is therefore given by a Hermite polynomial of order p multiplied by a Gaussian envelope: this exactly matches the results of the main text, obtained by starting from the series expansion of the thin-slab formula. Note the $\bar{\alpha}^p$ dependence, characterizing the perturbative regime.

[1] D. M. Villeneuve, Contemp. Phys. **59**, 47 (2018).
[2] M. Ferray, A. L'Huillier, X. F. Li, L. A. Lompre, G. Mainfray, and C. Manus, J. Phys. B **21**, L31 (1988).
[3] A. McPherson, G. Gibson, H. Jara, U. Johann, T. S. Luk, I. A. McIntyre, K. Boyer, and C. K. Rhodes, J. Opt. Soc. Am. B **4**, 595 (1987).
[4] M. Lewenstein, P. Balcou, M. Y. Ivanov, A. L'Huillier, and P. B. Corkum, Phys. Rev. A **49**, 2117 (1994).
[5] C.-G. Wahlström, J. Larsson, A. Persson, T. Starczewski, S. Svanberg, P. Salières, P. Balcou, and A. L'Huillier, Phys. Rev. A **48**, 4709 (1993).
[6] L. Rego, J. S. Román, L. Plaja, A. Picón, and C. Hernández-García, in *Vortex Dynamics and Optical Vortices*, edited by H. P. de Tejada (IntechOpen, Rijeka, Croatia, 2017), Chap. 9.
[7] R. W. Boyd, *Nonlinear Optics*, 3rd ed. (Academic Press, San Diego, 2008).
[8] D. D. Hickstein, F. J. Dollar, P. Grychtol, J. L. Ellis, R. Knut, C. Hernández-García, D. Zusin, C. Gentry, J. M. Shaw, T. Fan, K. M. Dorney, A. Becker, A. Jaroń-Becker, H. C. Kapteyn, M. M. Murnane, and C. G. Durfee, Nat. Photonics **9**, 743 (2015).
[9] F. Kong, C. Zhang, F. Bouchard, Z. Li, G. G. Brown, D. H. Ko, T. J. Hammond, L. Arissian, R. W. Boyd, E. Karimi, and P. B. Corkum, Nat. Commun. **8**, 14970 (2017).
[10] D. Gauthier, P. R. Ribič, G. Adhikary, A. Camper, C. Chappuis, R. Cucini, L. F. Dimauro, G. Dovillaire, F. Frassetto, R. Géneaux, P. Miotti, L. Poletto, B. Ressel, C. Spezzani, M. Stupar, T. Ruchon, and G. de Ninno, Nat. Commun. **8**, 14971 (2017).
[11] C. Chappuis, D. Bresteau, T. Auguste, O. Gobert, and T. Ruchon, Phys. Rev. A **99**, 033806 (2019).
[12] M. A. Khokhlova and V. V. Strelkov, New J. Phys. **22**, 093030 (2020).
[13] W. Komatsubara, F. Kong, C. Zhang, and P. B. Corkum, J. Phys. B **53**, 094002 (2020).
[14] D. H. Ko, G. G. Brown, C. Zhang, and P. B. Corkum, Optica **8**, 1632 (2021).
[15] X. Zhang, B. Shen, L. Zhang, and Y. Shi, High Power Laser Sci. Eng. **9**, e28 (2021).
[16] S. Jiang, M. Kowalewski, and K. E. Dorfman, Opt. Express **29**, 4746 (2021).
[17] C. Zhang, S. B. Schoun, C. M. Heyl, G. Porat, M. B. Gaarde, and J. Ye, Phys. Rev. Lett. **125**, 093902 (2020).
[18] S. Bengtsson and J. Mauritsson, J. Phys. B **52**, 063002 (2019).
[19] J. B. Bertrand, H. J. Wörner, H.-C. Bandulet, E. Bisson, M. Spanner, J.-C. Kieffer, D. M. Villeneuve, and P. B. Corkum, Phys. Rev. Lett. **106**, 023001 (2011).
[20] L. Li, P. Lan, L. He, X. Zhu, J. Chen, and P. Lu, Phys. Rev. Lett. **120**, 223203 (2018).
[21] M. Vimal, M. Luttmann, T. Gadeyne, M. Guer, R. Cazali, D. Bresteau, F. Lepetit, O. Tcherbakoff, J.-F. Hergott, T. Auguste, and T. Ruchon, companion paper, Phys. Rev. Lett. **131**, 203402 (2023).

[22] A. E. Siegman, *Lasers* (University Science Books, Sausalito, 1986).
[23] M. Lewenstein, P. Salières, and A. L'Huillier, Phys. Rev. A **52**, 4747 (1995).
[24] F. Aguillon, IEEE J. Quantum Electron. **25**, 917 (1989).
[25] T. Hasegawa and T. Shimizu, Opt. Commun. **160**, 103 (1999).
[26] L. Allen, M. W. Beijersbergen, R. J. C. Spreeuw, and J. P. Woerdman, Phys. Rev. A **45**, 8185 (1992).
[27] L. Rego, J. S. Román, A. Picón, L. Plaja, and C. Hernández-García, Phys. Rev. Lett. **117**, 163202 (2016).
[28] T. Wulle and S. Herminghaus, Phys. Rev. Lett. **70**, 1401 (1993).
[29] R. Géneaux, C. Chappuis, T. Auguste, S. Beaulieu, T. T. Gorman, F. Lepetit, L. F. DiMauro, and T. Ruchon, Phys. Rev. A **95**, 051801(R) (2017).
[30] W. T. Buono, A. Santos, M. R. Maia, L. J. Pereira, D. S. Tasca, K. Dechoum, T. Ruchon, and A. Z. Khoury, Phys. Rev. A **101**, 043821 (2020).
[31] A. T. O'Neil and J. Courtial, Opt. Commun. **181**, 35 (2000).